# Influence of the electrode-electrolyte interface on electrochemical CO2 reduction reaction and hydrogen evolution reaction

Ye, C.

# Chapter 5

# Electrolyte Effect on the Electrochemical $CO_2$ Reduction on Copper Gas Diffusion Electrodes

**Abstract:** The electrochemical reduction of $CO_2$ ($CO_2RR$) to multicarbon products at high current density over long electrolysis times remains an important challenge for implementation of this technology. In addition to neutral and alkaline media, recent works has shown that $CO_2RR$ to multicarbon products can also be achieved in highly acidic media (pH < 1). In this work, we investigate the influence of bulk electrolyte pH on $CO_2RR$ product distribution by studying the $CO_2RR$ product distribution on a copper gas diffusion electrode (Cu GDE) in a traditional bicarbonate electrolyte and a mildly acidic electrolyte in the presence of the same concentration of cations as in the bicarbonate electrolyte. We show that different $CO_2RR$ product distributions were only observed at low total applied current densities. Our results indicate that the selectivity of $CO_2RR$ on the copper GDE is independent of bulk pH and anions of the electrolyte at high total applied current densities. SEM images, along with EDX elemental mapping, indicate a less stable catalyst layer of the Cu GDE, resulting in electrode degradation over long electrolysis in acidic media compared to that in the bicarbonate electrolyte. Our work thereby confirms the importance of local environment on $CO_2RR$ and offers a more comprehensive understanding of $CO_2RR$ on Cu GDE in acidic media.

## 5.1 Introduction

The electrochemical carbon dioxide reduction reaction ($CO_2RR$) has gained substantial interest in the last few decades for the sustainable production of chemicals and fuels by utilizing an abundant carbon feedstock and renewable electricity. The $CO_2RR$ can generate various products in aqueous media, including formic acid (HCOOH), carbon monoxide (CO), hydrocarbons, and alcohols, depending on the catalyst and the microenvironment.[1-4] Copper-based catalysts are the only catalysts which produce significant amounts of high-value multicarbon products such as ethylene and ethanol during $CO_2RR$.[5] Despite extensive effort of the scientific community, reducing $CO_2$ toward multicarbon products with high activity and selectivity at low overpotentials remains challenging, which hinders the further industrial application of $CO_2RR$.[6]

In recent years, flow cells and gas diffusion electrodes (GDEs) have been employed to $CO_2RR$ electrolyzers. The porous structure of the GDE allows continuous $CO_2$ supply to the catalyst-electrolyte interface and therefore greatly improves local $CO_2$ concentration near the electrode during $CO_2RR$, enabling high current densities even at ambient conditions.[6-11]

In addition to the cell and GDE design, the nature of the catalysts as well as the electrolyte composition have been shown to play important roles in the $CO_2RR$. Highly alkaline potassium hydroxide electrolyte was found to improve the rate of C-C bond formation and facilitate production of $C_2H_4$.[12] However, rapid electrode degradation was observed in highly alkaline electrolyte,[9, 13] with one of the degradation mechanisms being $KHCO_3$ precipitation resulting from the reaction between $CO_2$ and KOH.[13-15] Other than the carbonate precipitation, such a reaction also leads to substantial $CO_2$ loss in the alkaline electrolyte and therefore greatly limits the carbon efficiency of the system.[7, 9-11]

To overcome these shortcomings, recently acidic electrolytes have been employed in $CO_2RR$ electrolyzers using flow cells and GDEs.[7, 9-11] Previous work has shown a CO faradaic efficiency of 80-90% on a gold GDE in pH 3 and 4 sulfate electrolyte.[7] In addition to a mildly acid electrolyte, strong acidic electrolyte (pH around 1) was employed with a Cu GDE

in flow cells.[10-11, 16] Although less $CO_2$ loss is expected in acidic electrolyte, different product distributions have been observed on Cu GDE.[10-11, 16] For example, FE of about 40% for hydrogen ($H_2$) and a total $C_{2+}$ FE of 40% were observed on a Cu GDE modified with a cation-augmenting layer,[10] CO and HCOOH were observed on Cu/C as main products at low overpotentials and FE with about 50% for $H_2$ at high overpotentials,[11] while a total FE of 83.7% for $C_{2+}$ products was observed on electrochemically reduced porous Cu nanosheets.[16] The observed different product distribution may result from various aspects, for example, gas electrode preparation method, electrode composition, $CO_2$ flow rate or cell configuration. Therefore, it is difficult to assign the stable electrolysis demonstrated in these works to the acidic electrolytes. To elucidate this, more systematic work is needed to exclude factors other than the pH of the electrolyte.

In this work, we investigate the influence of electrolytes with different bulk pH on both the $CO_2$RR product distribution and long-term electrode durability. We show the different product distributions at low total applied current densities, i.e. $H_2$ and HCOOH as main products in a $CO_2$ saturated 0.5 M $KHCO_3$ electrolyte and HCOOH and CO as main products in a $CO_2$ saturated pH 3 electrolyte with a presence of 0.25 M $K_2SO_4$ at the total applied current densities of 10 and 50 mA $cm^{-2}$, and similar product distributions at high current densities. In addition, we observed continuous decay after 5 hours electrolysis in both electrolytes. SEM images and EDX elemental mapping of Cu GDEs after long term electrolysis suggests that, in addition to the carbonate precipitation and Fe poisoning, the unstable catalyst layer in acidic media contributes to the electrode degradation during long term electrolysis.

## 5.2 Experimental Section

**Materials and chemicals.** $KHCO_3$ (99.5%), $K_2SO_4$(>99%) and $H_2SO_4$ (95% in water) were purchased from Acros Organics. Cu nanoparticles (25 nm), Nafion (5 wt % in lower aliphatic alcohols and water) and Chelex were purchased from Sigma-Aldrich. Milli-Q water (resistivity >18.2 MΩ·cm, TOC < 5 ppb) was used for all experiments in this work.

**GDE preparation.** The gas diffusion layer (GDL) was prepared using a previously reported method.[7] The catalyst ink was prepared by suspending Cu nanoparticles in isopropanol and adding 380 ul of Nafion solution (final 15 wt % of the catalysts). The mixture was then sonicated for 0.5 h to obtain a well dispersed suspension. Finally, the suspension was under continuous stirring to keep the suspension well dispersed. In the meantime, the suspension was airbrushed on a 17 $cm^2$ GDL. The final GDE was obtained after air drying. A catalyst loading of 1 $mg/cm^2$ was calculated from the weight difference before and after airbrushing.

**Electrode characterization.** Scanning electron microscopy (SEM) was performed on an Apreo SEM equipped with an energy-dispersive X-ray (EDX) analyzer to characterize the GDEs. SEM images were obtained with an acceleration voltage of 10 kV and an electron beam current of 0.8 nA. EDX (Instruments X-MaxN 150 Silicon Drift detector) was used for elemental analysis. The quantification was performed in automatic mode, without providing external standards. The data is displayed in atomic percentage for easier visualization.

**Flow cell electrolysis.** The bulk electrolysis experiments were carried out with a commercial two-compartment flow cell with 10 $cm^2$ GDE (ElectroCell, Micro Flow Cell). A reinforced Nafion membrane N234 was used to separate the anode and the cathode. 0.5M $H_2SO_4$ solution was used as anolyte and a dimensionally stable anode (DSA®, ElectroCell) was used as anode for all measurements. pH of the electrolyte was adjusted with $H_2SO_4$ and a pH meter when necessary. The catholyte was $CO_2$ saturated 0.5M $KHCO_3$ or pH 3 0.25M $K_2SO_4$ electrolyte. The electrolytes were circulated in the compartments at a flow rate of 30 mL/min with a peristaltic pump, $CO_2$ was fed through the GDE in the cathodic compartment at a flow rate of 30 mL/min. Before each experiment, $CO_2$ was purged through electrolyte for 1 h to obtain a stable electrolyte prior to each $CO_2$RR experiment. The cell was controlled by an Autolab PGSTAT100N potentiostat and each current density was applied for an hour. The gas product analysis was performed with a gas chromatograph (Varian 4900 micro GC) equipped with four modules: COx module, MS5 (mol. sieve) module, PPQ (poraplotQ) module and 52C WAX module. Gaseous samples were taken from gas outlet every 3 minutes. The current efficiencies shown throughout this work represent the average values obtained at 36, 48 and

60 mins during 1 h of electrolysis, with the corresponding standard deviation. Liquid products were analyzed with High Performance Liquid Chromatograph (HPLC) with an Aminex HPX-87H (BioRad) and a RID detector (Shimadzu). For stability performance, a total applied current density of 200 mA $cm^{-2}$ was applied to the cell, with only gas products analyzed as an indicator of $CO_2$RR performance.

## 5.3 Results and Discussion

### 5.3.1 Results

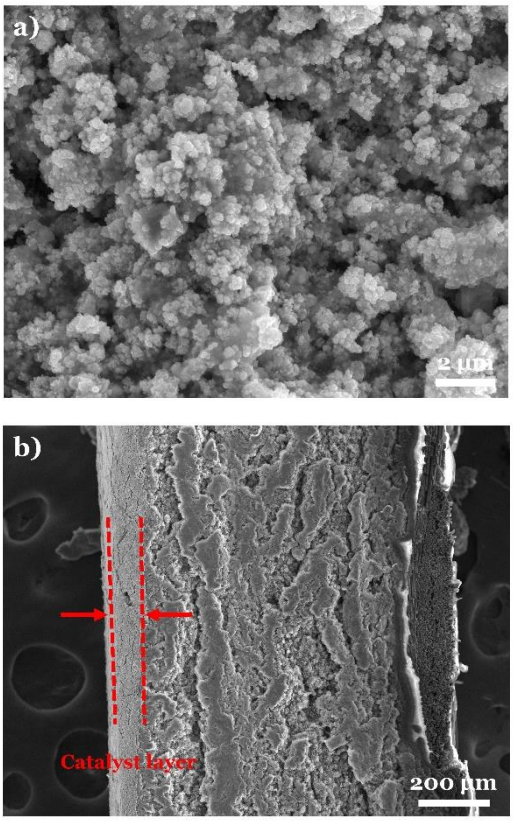


**Figure 5.1** SEM images of a) the surface catalyst and b) cross section of the Cu GDE before $CO_2$RR experiments.

Scanning electron microscopy was used to characterize the morphology of the Cu GDEs. Figures 5.1a and 1b show SEM images of the surface catalyst and a cross section of the Cu GDEs, respectively, prior to $CO_2$RR experiments. The Cu nanocatalysts are well dispersed on the surface of the GDE with a layer thickness of about 100 µm (the thickness of the catalyst

layer was confirmed with elemental analysis).

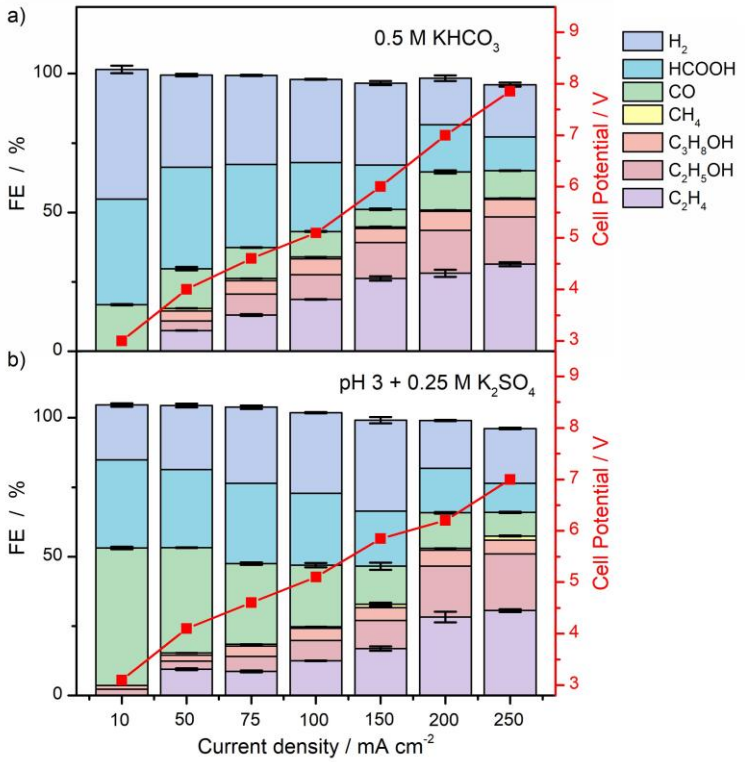


**Figure 5.2** Effect of bulk pH on $CO_2$RR performance. FEs of $H_2$, HCOOH, CO, $CH_4$, $C_3H_8OH$, $C_2H_5OH$ and $C_2H_4$ (left axis) as well as cell potential (right axis) as a function of total applied current density on Cu GDE in $CO_2$ saturated a) 0.5M $KHCO_3$ (pH 7.2) and b) pH 3 electrolyte with the presence of 0.25 M $K_2SO_4$ (pH 3.0).

To study the effect of bulk pH on $CO_2$RR, experiments were carried out in 0.5M $KHCO_3$ (bulk pH of 7.2 before electrolysis) and $CO_2$ saturated 0.25M $K_2SO_4$ (adjusted with $H_2SO_4$ to a bulk pH of 3 before electrolysis), respectively, where the cation concentrations were deliberately kept the same to exclude a bulk cation concentration effect on $CO_2$RR. Figure 5.2 shows the Faradaic efficiencies (FEs) for $CO_2$RR products as well as the cell potential in the two electrolytes as a function of total applied current density. As shown in Figure 5.2a, in 0.5M $KHCO_3$, $H_2$ and HCOOH are major products obtained during $CO_2$RR at low total applied current densities. Specifically, at 10 mA $cm^{-2}$, the FEs of $H_2$, HCOOH and CO are 46.6%, 38.1%, and 16.7% respectively. With increasing total applied current density, the FEs of $H_2$ and HCOOH decrease, while the total FE of CO and its further reduced products

increase. At the highest total applied current density of 250 mA $cm^{-2}$, the FEs of $H_2$ and HCOOH have reduced to 18.9% and 12.2% respectively, while the FEs of CO, $C_2H_4$, $C_2H_5OH$ and $C_3H_8OH$ are 9.9%, 31.4%, 17.3% and 6.3% respectively. These results agree well with previously reported findings for Cu nanoparticle-based GDEs in bicarbonate electrolyte.[17]

Figure 5.2b shows the $CO_2RR$ performance in the pH 3 sulfate electrolyte. At low total applied current densities (below 100 mA $cm^{-2}$), the primary products are HCOOH and CO. FEs of $H_2$, HCOOH and CO are 19.7%, 31.7%, and 49.6% respectively at 10 mA $cm^{-2}$. These results suggest that $H_2$ formation is inhibited at low total applied current densities under these working conditions. This might be explained with the model recently proposed by Bondue et. al.[18] According to their model, $OH^-$ generated from $CO_2RR$ could neutralize protons diffusing from bulk electrolyte to the catalyst surface to generate $H_2O$ in pH 3 electrolyte and thereby inhibits $H_2$ formation during $CO_2RR$.[18] This is in contrast with the $H_2$ production observed in 0.5M $KHCO_3$ at low current densities, where $HCO_3^-$ acts as proton donor and is readily reduced to produce $H_2$. Additionally, minor amounts of $C_2H_5OH$ and $C_3H_8OH$ are detected in the pH 3 electrolyte already at 10 mA $cm^{-2}$. With increasing total applied current density, the product distribution in the pH 3 electrolyte becomes similar to the one in 0.5 M $KHCO_3$, especially at 200 and 250 mA $cm^{-2}$. These results suggest that the selectivity of $CO_2RR$ on the Cu GDE remains consistent regardless of variations in pH or the composition of the bulk electrolyte at high total applied current densities.

The right axis of Figure 5.2 shows the cell potential obtained during $CO_2RR$ in the 0.5 M $KHCO_3$ and pH 3 sulfate electrolytes, respectively. As expected, the cell potential increases in both electrolytes with the increasing total applied current density. Furthermore, the cell potential in pH 3 sulfate electrolyte remains lower than the cell potential in 0.5 M $KHCO_3$. This is likely due to the higher ionic conductivity of the pH 3 electrolyte. (Specifically, the ionic conductivity of $1.167 \times 10^{-1}$ S $cm^{-1}$ in pH 3 with the presence of 0.25M $K_2SO_4$ is higher than the ionic conductivity of $5.895 \times 10^{-2}$ S $cm^{-1}$ in 0.5 M $KHCO_3$ despite the subtle electrolyte component change which occurs after $CO_2$ saturation.)

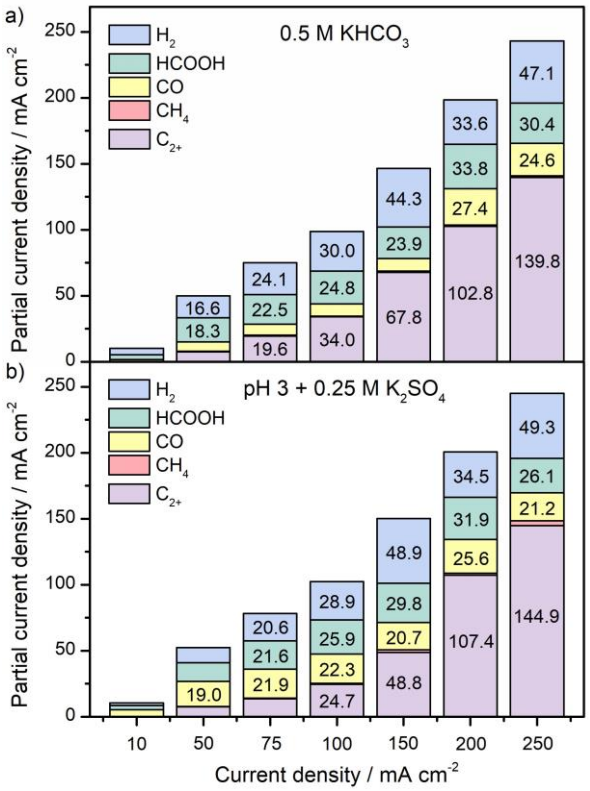


**Figure 5.3** Partial current densities of $H_2$, HCOOH, CO, $CH_4$ and $C_{2+}$ products ($C_3H_8OH$, $C_2H_5OH$ and $C_2H_4$) as a function of total applied current density on Cu GDE in $CO_2$ saturated a) 0.5M $KHCO_3$ (pH 7.2) and b) 0.25M $K_2SO_4$ (pH 3.0).

Figure 5.3 shows the partial current densities of each $CO_2$RR product in both electrolytes. It clearly shows higher CO production in pH 3 electrolyte for lower total applied current densities, and similar product distributions in both electrolytes at higher total applied current densities. We ascribe this to the local pH regulation which is different between these two electrolytes at these lower current densities.

To study the stability of both electrolysis systems, long term electrolysis of $CO_2$RR at a total applied current density of 200 mA $cm^{-2}$ was performed on the Cu GDE in both electrolytes. The FE of $C_2H_4$ and the cell potential were chosen as indicators of $CO_2$RR performance. Left and right axis of Figure 5.4 shows FE of $C_2H_4$ (solid symbols) and cell potential (hollow symbols), respectively, as a function of time, in 0.5 $KHCO_3$ (green) and pH 3 electrolyte with presence of 0.25 M $K_2SO_4$ (pink). The results show that the cell potential in 0.5M $KHCO_3$ is more stable than in the pH 3 electrolyte. On the other hand, the FE of $C_2H_4$ in pH 3

electrolyte remains higher than in 0.5 M $KHCO_3$ for 14 hours (and especially for the first 8 hours).

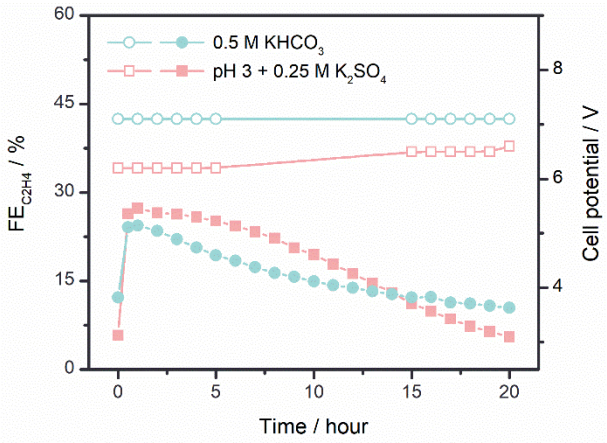


**Figure 5.4** Comparison of $CO_2RR$ performance at a total applied current density of 200 mA $cm^{-2}$ on a Cu GDE in neutral and acidic bulk electrolyte: solid symbols representing FE of $C_2H_4$ corresponding to left axis and hollow symbols representing cell potential corresponding to right axis. Electrolytes: 0.5 $KHCO_3$ (green) and pH 3 electrolyte with presence of 0.25M $K_2SO_4$ (pink).

These results suggest that although less $KHCO_3$ precipitation is expected in pH 3 electrolyte, it does not necessarily lead to stable $CO_2RR$ performance during long term electrolysis. Considering the fact that bulk pH before and after $CO_2RR$ electrolysis remain relatively stable (see Table S1) and $CO_2RR$ performance derived from long term electrolysis slowly went down over time, we assume that the loss of $CO_2RR$ activity likely stems from electrode degradation during long term electrolysis.

To test our hypothesis, copper GDEs were characterized after long term electrolysis. The copper GDEs were rinsed with Milli-Q water at least three times and dried in the air immediately after long term electrolysis. Next, they were kept in sealed sample bags prior to SEM characterization. Figure 5.5 shows the characterization of copper GDEs after 20 hours electrolysis at a total applied current density of 200 mA $cm^{-2}$ in 0.5M $KHCO_3$ and pH 3 sulfate electrolytes, respectively. Figure 5.5a, b show that surface catalysts remain as nanoparticles after long term $CO_2RR$ experiments in both electrolytes. Figures 5.5c, d show

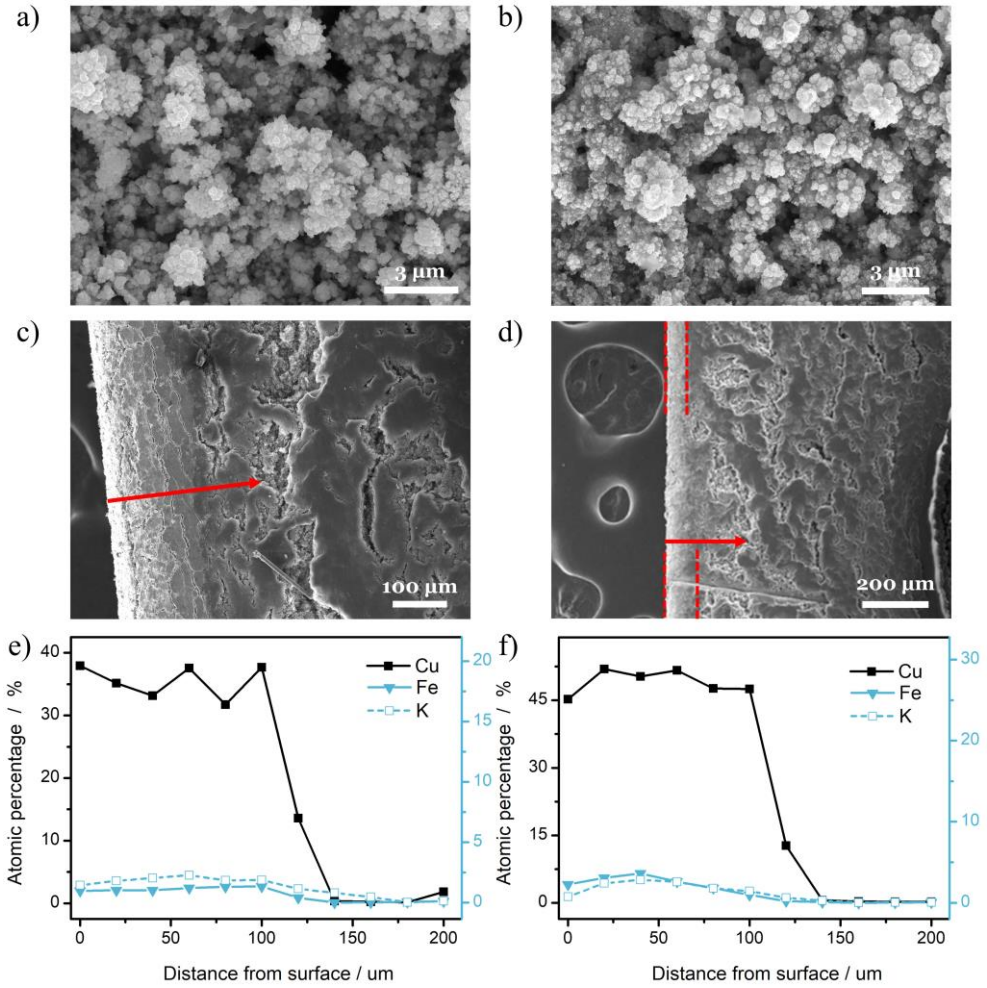


**Figure 5.5** Characterization of copper GDEs after 20 hours long term electrolysis at a total applied current density of 200 mA $cm^{-2}$. a) Surface catalyst morphology, c) cross section and e) atomic percentages of Cu, K, Fe as a function of distance from top surface of catalyst layer obtained from EDX elemental mapping of a copper GDE after long term electrolysis in $CO_2$ saturated 0.5 M $KHCO_3$; b) Surface catalyst morphology, d) cross section and f) atomic percentages of element Cu, K, Fe as a function of distance from top surface of catalyst layer obtained from EDX elemental mapping of a copper GDE after long term electrolysis in $CO_2$ saturated pH 3 electrolyte with presence of 0.25 M $K_2SO_4$.

the cross section of the Cu GDEs after long term electrolysis in 0.5M $KHCO_3$ and 0.25M $K_2SO_4$ electrolytes, respectively. Figure 5.5c shows a well-preserved catalyst layer (around 100 µm) on GDE after long term electrolysis in 0.5 M $KHCO_3$. On the other hand, it appears that the catalyst layer on copper GDE after long term electrolysis in pH 3 $K_2SO_4$ electrolyte was less intact, as shown by different distances between dashed lines in Figure 5.5d, which is

obtained from EDX mapping and indicates different thickness of the catalyst layer at different locations of the GDE. Supporting Figures D.1 and D.2 show further SEM images of the Cu GDE with catalyst layers of less than 50 μm and images of copper GDEs with a black deposit on the current collector respectively, which suggests a redeposition of Cu nanoparticles on the current collector during $CO_2$RR in the pH 3 electrolyte. In addition to the loss of Cu nanoparticles, the presence of $KHCO_3$ precipitation and Fe deposition originally from current collector (steel) in the catalyst layer are often considered as common reasons for causing loss of $CO_2$RR activity. Therefore, the atomic percentages of Cu (left axis), Fe (right axis) and K (right axis) obtained from EDX mapping along the arrow indicted in Figures 5.5c, d were obtained and are shown in Figure 5.5e, f respectively, with the positions chosen to have similar thicknesses of the catalyst layer. Figure 5.5e shows the presence of K throughout the catalyst layer as well as traces of Fe. In contrast, Figure 5.5f shows the presence of elements K and Fe in the top part of the catalyst layer. Additionally, it is worth noting that element Fe is higher on copper GDE after electrolysis in pH 3 sulfate electrolyte than on copper GDE after electrolysis in 0.5 M $KHCO_3$ in view of the ratio of atomic level of Fe and Cu in each GDE, which suggests more Fe deposition on the catalyst layer in pH 3 sulfate electrolyte under our working conditions.

### 5.3.2 Discussion

Our work shows that operating in acidic media is a promising method to decrease the $CO_2$ consumption caused by electrolyte without harming other important figures of merit such as the product distribution and electrode stability. Specifically, total FEs of $CO_2$RR products reach 80% on Cu GDE at total applied current densities of 200 and 250 mA $cm^{-2}$ in both electrolytes. In the meantime, similar $CO_2$RR product distributions were observed under these conditions. However, electrolytes with different bulk pH affect the $CO_2$RR product distribution at low total applied current densities. In pH 3 electrolyte, CO and HCOOH are the main products, while $H_2$ and HCOOH are more pronounced in 0.5 M $KHCO_3$, at the total applied current densities of 10 and 50 mA $cm^{-2}$. Additionally, minor $C_{2+}$ products were observed in pH 3 electrolyte at a total applied current density of 10 mA $cm^{-2}$.

Previous work has shown that the selectivity and activity of a catalyst is highly sensitive to local pH[19-23] and cations[24-27]. Numerous experimental studies have shown that higher local pH conditions promote CO and multi-carbon products while suppressing $H_2$ and $CH_4$ on Cu catalysts.[12, 20-23] In addition to the pH of the bulk electrolyte, buffer capacity of the electrolyte also plays an import role on the local pH during $CO_2RR$.[8, 22-23, 28] Liu et al shows dramatic change of local pH in low buffered electrolytes with a rotating ring-disk electrode.[28] Burdyny et al investigated the pH near the GDE as a function of total applied current density during $CO_2RR$ in commonly-used electrolytes, namely 0.1M $KHCO_3$, 1M $KHCO_3$ and 1M KCl, with a 1D reaction-diffusion model.[8] The modelling shows a sudden increase of the local pH in the electrolytes with low buffer capacities at low current densities, which thereby leads to a high local pH in the low buffered electrolyte, and a similar ultimate alkaline local pH in all electrolytes (except a high local pH in high alkaline electrolyte) at high total applied current densities.[8]

These observations are in line with our experimental results. Considering the same cation concentration in both electrolytes and electrodes with the same preparation method in the present work, the observed different product distribution at low total applied current densities must be due to different local environment at the interface resulting from electrolyte. At low total applied current densities, $HCO_3^-$ acts as a buffer species and a proton donor contributing to the $H_2$ production in 0.5 M $KHCO_3$. On the other hand, the rapidly increased local pH at the interface in low buffered pH 3 electrolyte leads to an inhibition of $H_2$ production because of the sluggish kinetics for water reduction in alkaline conditions. Under high total applied current densities, highly alkaline local environments at the interface are achieved, where $HCO_3^-$ is consumed by excess $OH^-$ formed during $CO_2RR$ and no long acts as buffer at the interface. Consequently, a similar local environment at the interface is expected in both electrolytes. Therefore, a similar products distribution in both electrolytes are observed.

Although alkaline local environments at the interface are unavoidable in both electrolytes, less carbonate/bicarbonate are expected during the reaction as the bulk protons can to some extent neutralize the $OH^-$ produced upon $CO_2RR$ while in alkaline media both $OH^-$ originated

from bulk electrolyte and generated from $CO_2$RR will be neutralized by $CO_2$. Our results shows that $K^+$, which corresponds to carbonate/bicarbonate formation, is present in the catalysts layer after long term electrolysis in 0.5M $KHCO_3$ at a slightly higher level than in pH 3 electrolyte. In addition to $K^+$, a higher content of Fe element, which is considered as metal impurity,[15, 29] was observed on copper GDE after long term electrolysis in pH 3 electrolyte compared to 0.5M $KHCO_3$ electrolyte. This may be related to the higher instability of the current collector under acid conditions. However, the observed elemental difference does not seem high enough to explain $CO_2$RR performance over long term, as shown in Figure 5.4.

SEM characterization and EDX elemental mapping suggests a less stable catalyst layer in pH 3 electrolyte, which may be another factor contributing to the drop in $CO_2$RR performance in pH 3 electrolyte. It is known that Cu can be easily oxidized at open circuit potential. The formed Cu oxide dissolves in the acidic media and may be subsequently reduced back to Cu during electrolysis, which thereby leads to a less stable catalyst layer over long term electrolysis in pH 3 electrolyte. Further, this could also explain the black deposition on current collector after electrolysis. Therefore, we show the unavoidable interactions between the acidic reagent and the commonly used compartments, e.g. GDE, may result in inherently unstable $CO_2$RR electrolyzers.

## 5.4 Conclusions

In summary, we show that operating $CO_2$RR in acidic media is a promising approach to lower the $CO_2$ consumption and improve the energy efficiency without compromising the selectivity toward $C_{2+}$ products. Compared with commonly used bicarbonate electrolytes, our results in mild acidic electrolyte show an inhibition of $H_2$ production at low total applied current densities and similar $CO_2$RR product distribution at high total applied current densities. The similar $CO_2$RR product distributions at high total applied current densities in both electrolytes indicate a similar local pH at the interface under these conditions. In addition, our result shows the unavoidable interaction between the acidic electrolyte and Cu oxide may result in inherently unstable Cu catalyst layer on GDE. Our work thereby offers

new insights of $CO_2RR$ in acidic media and points out the new challenge of employing acidic media in $CO_2RR$ electrolyzers.

## References

1. Kuhl, K. P.; Cave, E. R.; Abram, D. N.; Jaramillo, T. F., New insights into the electrochemical reduction of carbon dioxide on metallic copper surfaces. *Energy Environ. Sci.* **2012,** *5* (5), 7050-7059.
2. Hatsukade, T.; Kuhl, K. P.; Cave, E. R.; Abram, D. N.; Jaramillo, T. F., Insights into the electrocatalytic reduction of $CO_2$ on metallic silver surfaces. *Phys. Chem. Chem. Phys.* **2014,** *16* (27), 13814-9.
3. Min, X.; Kanan, M. W., Pd-catalyzed electrohydrogenation of carbon dioxide to formate: high mass activity at low overpotential and identification of the deactivation pathway. *J. Am. Chem. Soc.* **2015,** *137* (14), 4701-8.
4. Cave, E. R.; Montoya, J. H.; Kuhl, K. P.; Abram, D. N.; Hatsukade, T.; Shi, C.; Hahn, C.; Norskov, J. K.; Jaramillo, T. F., Electrochemical $CO_2$ reduction on Au surfaces: mechanistic aspects regarding the formation of major and minor products. *Phys. Chem. Chem. Phys.* **2017,** *19* (24), 15856-15863.
5. De Luna, P.; Hahn, C.; Higgins, D.; Jaffer, S. A.; Jaramillo, T. F.; Sargent, E. H., What would it take for renewably powered electrosynthesis to displace petrochemical processes? *Science* **2019,** *364* (6438).
6. Philips, M. F.; Gruter, G.-J. M.; Koper, M. T. M.; Schouten, K. J. P., Optimizing the Electrochemical Reduction of $CO_2$ to Formate: A State-of-the-Art Analysis. *ACS Sustainable Chemistry & Engineering* **2020,** *8* (41), 15430-15444.
7. Monteiro, M. C. O.; Philips, M. F.; Schouten, K. J. P.; Koper, M. T. M., Efficiency and selectivity of $CO_2$ reduction to CO on gold gas diffusion electrodes in acidic media. *Nat. Commun.* **2021,** *12* (1), 1-7.
8. Burdyny, T.; Smith, W. A., $CO_2$ reduction on gas-diffusion electrodes and why catalytic performance must be assessed at commercially-relevant conditions. *Energy Environ. Sci.* **2019,** *12* (5), 1442-1453.
9. Zhang, X.; Li, J.; Li, Y. Y.; Jung, Y.; Kuang, Y.; Zhu, G.; Liang, Y.; Dai, H., Selective and High Current $CO_2$ Electro-Reduction to Multicarbon Products in Near-Neutral KCl Electrolytes. *J. Am. Chem. Soc.* **2021,** *143* (8), 3245-3255.
10. Huang, J. E.; Li, F.; Ozden, A.; Sedighian Rasouli, A.; Garcia de Arquer, F. P.; Liu, S.; Zhang, S.; Luo, M.; Wang, X.; Lum, Y.; Xu, Y.; Bertens, K.; Miao, R. K.; Dinh, C. T.; Sinton, D.; Sargent, E. H., $CO_2$ electrolysis to multicarbon products in strong acid. *Science* **2021,** *372* (6546), 1074-1078.
11. Gu, J.; Liu, S.; Ni, W.; Ren, W.; Haussener, S.; Hu, X., Modulating electric field distribution by alkali cations for $CO_2$ electroreduction in strongly acidic medium. *Nat. Catal.* **2022,** *5* (4), 268-276.
12. Dinh, C. T.; Burdyny, T.; Kibria, M. G.; Seifitokaldani, A.; Gabardo, C. M.; Garcia de Arquer, F. P.; Kiani, A.; Edwards, J. P.; De Luna, P.; Bushuyev, O. S.; Zou, C.; Quintero-Bermudez, R.; Pang, Y.; Sinton, D.; Sargent, E. H., $CO_2$ electroreduction to ethylene via hydroxide-mediated copper catalysis at an abrupt interface. *Science* **2018,** *360* (6390), 783-787.
13. Popović, S.; Smiljanić, M.; Jovanovič, P.; Vavra, J.; Buonsanti, R.; Hodnik, N., Stability and degradation mechanisms of copper-based catalysts for electrochemical $CO_2$ reduction. *Angew. Chem.* **2020,** *132* (35), 14844-14854.
14. Rabinowitz, J. A.; Kanan, M. W., The future of low-temperature carbon dioxide electrolysis depends on solving one basic problem. *Nat. Commun.* **2020,** *11* (1), 5231.
15. Nwabara, U. O.; Cofell, E. R.; Verma, S.; Negro, E.; Kenis, P. J. A., Durable Cathodes and

Electrolyzers for the Efficient Aqueous Electrochemical Reduction of $CO_2$. *ChemSusChem* **2020,** *13* (5), 855-875.

16. Ma, Z.; Yang, Z.; Lai, W.; Wang, Q.; Qiao, Y.; Tao, H.; Lian, C.; Liu, M.; Ma, C.; Pan, A.; Huang, H., $CO_2$ electroreduction to multicarbon products in strongly acidic electrolyte via synergistically modulating the local microenvironment. *Nat. Commun.* **2022,** *13* (1), 7596.

17. Ma, M.; Clark, E. L.; Therkildsen, K. T.; Dalsgaard, S.; Chorkendorff, I.; Seger, B., Insights into the carbon balance for $CO_2$ electroreduction on Cu using gas diffusion electrode reactor designs. *Energy Environ. Sci.* **2020,** *13* (3), 977-985.

18. Bondue, C. J.; Graf, M.; Goyal, A.; Koper, M. T. M., Suppression of Hydrogen Evolution in Acidic Electrolytes by Electrochemical $CO_2$ Reduction. *J. Am. Chem. Soc.* **2021,** *143* (1), 279-285.

19. Schouten, K. J. P.; Pérez Gallent, E.; Koper, M. T. M., The influence of pH on the reduction of CO and $CO_2$ to hydrocarbons on copper electrodes. *J. Electroanal. Chem.* **2014,** *716*, 53-57.

20. Lim, C. F. C.; Harrington, D. A.; Marshall, A. T., Effects of mass transfer on the electrocatalytic $CO_2$ reduction on Cu. *Electrochim. Acta* **2017,** *238*, 56-63.

21. Pander, J. E.; Ren, D.; Huang, Y.; Loo, N. W. X.; Hong, S. H. L.; Yeo, B. S., Understanding the Heterogeneous Electrocatalytic Reduction of Carbon Dioxide on Oxide - Derived Catalysts. *ChemElectroChem* **2017,** *5* (2), 219-237.

22. Kas, R.; Kortlever, R.; Yılmaz, H.; Koper, M. T. M.; Mul, G., Manipulating the Hydrocarbon Selectivity of Copper Nanoparticles in $CO_2$ Electroreduction by Process Conditions. *ChemElectroChem* **2014,** *2* (3), 354-358.

23. Varela, A. S.; Kroschel, M.; Reier, T.; Strasser, P., Controlling the selectivity of $CO_2$ electroreduction on copper: The effect of the electrolyte concentration and the importance of the local pH. *Catal. Today* **2016,** *260*, 8-13.

24. Resasco, J.; Chen, L. D.; Clark, E.; Tsai, C.; Hahn, C.; Jaramillo, T. F.; Chan, K.; Bell, A. T., Promoter Effects of Alkali Metal Cations on the Electrochemical Reduction of Carbon Dioxide. *J. Am. Chem. Soc.* **2017,** *139* (32), 11277-11287.

25. Singh, M. R.; Kwon, Y.; Lum, Y.; Ager, J. W., 3rd; Bell, A. T., Hydrolysis of Electrolyte Cations Enhances the Electrochemical Reduction of $CO_2$ over Ag and Cu. *J. Am. Chem. Soc.* **2016,** *138* (39), 13006-13012.

26. Perez-Gallent, E.; Marcandalli, G.; Figueiredo, M. C.; Calle-Vallejo, F.; Koper, M. T. M., Structure- and Potential-Dependent Cation Effects on CO Reduction at Copper Single-Crystal Electrodes. *J. Am. Chem. Soc.* **2017,** *139* (45), 16412-16419.

27. Ayemoba, O.; Cuesta, A., Spectroscopic Evidence of Size-Dependent Buffering of Interfacial pH by Cation Hydrolysis during $CO_2$ Electroreduction. *ACS Appl. Mater. Interfaces* **2017,** *9* (33), 27377-27382.

28. Liu, X.; Monteiro, M. C. O.; Koper, M. T. M., Interfacial pH measurements during $CO_2$ reduction on gold using a rotating ring-disk electrode. *Phys. Chem. Chem. Phys.* **2023,** *25* (4), 2897-2906.

29. Wuttig, A.; Surendranath, Y., Impurity Ion Complexation Enhances Carbon Dioxide Reduction Catalysis. *ACS Catal.* **2015,** *5* (7), 4479-4484.